IEEE Access
Multidisciplinary | Rapid Review | Open Access Journal

Received 21 September 2023, accepted 4 October 2023, date of publication 9 October 2023, date of current version 12 October 2023.

Digital Object Identifier 10.1109/ACCESS.2023.3322730

RESEARCH ARTICLE

Low-Profile Four-Port MIMO Antenna Module Based 16-Port Closely-Spaced 2 × 2 Module Array for 6G Upper Mid-Band Mobile Devices

KIN-LU WONG[1,2], (Fellow, IEEE), SHAO-EN HONG[1], (Student Member, IEEE), AND WEI-YU LI[3], (Member, IEEE)

[1]Department of Electrical Engineering, National Sun Yat-sen University, Kaohsiung 80424, Taiwan
[2]6G Communication and Sensing Research Center, National Sun Yat-sen University, Kaohsiung 80424, Taiwan
[3]Information and Communications Research Laboratories, Industrial Technology Research Institute, Hsinchu 31057, Taiwan

Corresponding author: Kin-Lu Wong (wongkl@mail.nsysu.edu.tw)

This work was supported in part by the National Science and Technology Council, Taiwan, under Grant NSTC 112-2218-E-110-004.

ABSTRACT The next six-generation (6G) mobile device is expected to support eight MIMO spatial streams to achieve a much larger spectral efficiency than the current fifth-generation (5G) 4 × 4 MIMO operation in the mid-band such as the 3.5 GHz band. Thus, for the expected 6G higher-order MIMO operation in the new possible upper mid-band of 7.025-8.4 GHz, the mobile device should have at least eight embedded MIMO antennas. However, owing to the limited space inside the mobile device, embedding a large number of MIMO antennas is a great challenge. In this article, we present a 16-port closely-spaced 2 × 2 module array formed by four low-profile (thickness 0.9 mm) four-port MIMO antenna modules covering 7.025-8.4 GHz for the mobile device to support up to 16 × 8 MIMO operation (16 receive antennas for 8 spatial streams). With an extreme or a much larger number of the receive antennas than that of the incoming spatial streams, it is denoted here as the extreme receive antennas (ERA)-aided MIMO for enhanced performance. The 16-port 2 × 2 module array can fit in a mobile device such as in the backcover region of the modern smartphone. The fabricated module array was applied as 16 receive antennas in the 16 × 8 MIMO system with 8 spatial streams to achieve a high spectral efficiency of about 56 bps/Hz, which is larger than three times that (about 16 bps/Hz) of the 5G 4 × 4 MIMO operation in the 3.5 GHz band. Also, in term of the obtained spectral efficiency, the 16 × 8 MIMO system outperforms the 8 × 8 MIMO system in which about 34 bps/Hz is reported. Details of the proposed 16-port closely-spaced module array and the measured 16 × 8 MIMO system performance are presented.

INDEX TERMS 6G upper mid-band, 16 × 8 MIMO systems, mobile antennas, MIMO antennas, MIMO antenna modules, closely-spaced module arrays, extreme receive antennas (ERA)-aided MIMO.

I. INTRODUCTION

For 6G communications, the multi-input-multi-output (MIMO) operation for the mobile device or the user-experienced MIMO is envisioned to support at least 8 spatial streams [1] to achieve a much larger spectral efficiency than that for 5G communications supporting 4 spatial streams. In addition, following the same carrier bandwidth evolution from 4G with 20 MHz to 5G with 100 MHz (5 times increase), 6G is expected to use 500 MHz [2] or 400 MHz and beyond [3]. In this case, the 5G user with 4 × 4 MIMO and 100 MHz bandwidth in the mid-band can experience larger than 1 Gbps throughput. On the other hand, the 6G user with the higher-order (at least 8 × 8) MIMO and at least 400 MHz bandwidth is promising to experience larger than 10 Gbps throughput [1], [2], [3].

In order to support the 6G vision, the required MIMO antennas in the mobile device should be at least doubled as compared to those applied in the 5G mobile device. However, since the mobile device generally has a compact structure, there is limited space available for the internal antennas. To embed a large number of required MIMO antennas in the future 6G mobile device is therefore very challenging.

The associate editor coordinating the review of this manuscript and approving it for publication was Ravi Kumar Gangwar.

It is also worthy to note that new frequency spectrum for 6G will be introduced. The upper mid-band of 7-24 GHz [1], [3], [4], [5], [6] between the 5G mid-band (3.3-5.0 GHz) and 5G high-band (24-52 GHz) is a very promising one for 6G applications. This is because the upper mid-band is expected to have faster speeds and wider coverage than the 5G high-band or millimeter-wave operation [5].

Additionally, in the possible frequency band in the upper mid-band, the lower frequencies close to the mid-band, such as the 7.025-7.125 GHz (a possible new global mobile communication band [7]) and 7.125-8.4 GHz (the operating band of interest to future mobile communications given that it is close to the 5G mid-band [8]) are especially recommended. This is mainly because the lower frequencies in the upper mid-band have longer wavelengths and can experience less propagation path loss for wider coverage, which is an important issue for mobile communications.

Recently, the capability of the upper mid-band to support rich multipath scattering for higher-order MIMO operation has also been investigated [9]. Promising results have been reported that in the possible new frequency band of 7.025-7.125 GHz (7.1 GHz band) for the global mobile communication spectrum [7], the 8 × 8 MIMO operation can support the signal modulation of 64 Quadrature Amplitude Modulation (QAM) with 6 bits per symbol to achieve a spectral efficiency of about 34 bps/Hz [9]. This suggests that with a carrier bandwidth of 400 MHz [3], the user can experience a data throughput of larger than 10 Gbps.

However, the study in [9] did not include the use case of hand holding. With the user's hand holding the mobile device such as the smartphone studied in the 3.5 GHz band [10], the signal noise ratios of the MIMO antennas inside the smartphone are expected to decrease, which will lead to degraded MIMO performance. In the upper mid-band such as the 7.1 GHz band [8], the user's hand holding the mobile device may cause similar or even more seriously degraded MIMO performance. This is because the relatively higher frequencies of the 7.1 GHz band than those of the 5G mid-band such as the 3.5 GHz band. In this case, it is very likely that the 8 × 8 MIMO operation can no longer support the 64 QAM (6 bits per symbol) signal modulation, thereby leading to a decreased spectral efficiency.

To alleviate the user's hand holding effect and also to provide a more stable higher-order MIMO operation with 8 spatial streams in the future 6G upper mid-band application, we propose to use 16 receive antennas in the mobile device for the 8 spatial streams. That is, the 16 × 8 MIMO operation for the 6G mobile device is proposed. The use of an extreme or a much larger number of the receive antennas than that of the incoming spatial streams is denoted here as the extreme receive antennas (ERA)-aided MIMO for the mobile device. By applying the ERA-aided MIMO at the device side, similar to the extreme massive MIMO proposed at the base station side [3], [6], enhanced MIMO performance is expected.

With the receive antennas to be two times that of the spatial streams, it is expected that the 16 × 8 MIMO operation can support a higher signal modulation than that (64 QAM) in the 8 × 8 MIMO system [10]. That is, the 16 × 8 MIMO operation is promising to support at least 256 QAM (8 bits per symbol), even with the scenario of the user's hand holding the mobile device. In this case, a larger spectral efficiency (about 33% larger for using 256 QAM with respect to using 64 QAM) can be obtained for the MIMO operation with 8 spatial streams for the user. This can in turn lead to a much larger user-experienced data throughput.

Thus, in order to easily embed 16 MIMO antennas in the mobile device such as the smartphone, we present in this study a 16-port closely-spaced 2 × 2 module array formed by four low-profile (thickness 0.9 mm) four-port MIMO antenna modules covering 7.025-8.4 GHz [7], [8] for 16 × 8 MIMO applications. The 16-port module array has a very low profile of 0.9 mm and a small size of 65 mm × 65 mm (about 1.5λ × 1.5λ at 7.025 GHz). The low profile and small size allow it to fit in the narrow backcover region (typically less than 1 mm spacing between the backcover and the battery/electronic modules and about 70 mm × 150 mm in area) of the modern smartphone [9], [11], [12], [13], [14], [15].

In addition, the 2 × 2 module array with 16 MIMO antennas integrated therein can generate 16 uncorrelated waves with very low envelope correlation coefficients (ECCs $\ll 0.1$) over the operating band of 7.025-8.4 GHz. The 16 uncorrelated waves are two times that (8 waves) in [9] and [11], three times that (6 waves) in [12] and four times that (4 waves) in [13], [14] and [15] for the backcover MIMO antenna application in the smartphone.

It is also worthy to note that each low-profile four-port antenna module in the array has a small size of 31 mm × 31 mm (0.73λ × 0.73λ at 7.025 GHz) and is spaced by a small distance of 3 mm (only about 0.07λ at 7.025 GHz) to its nearby modules. The small size of the four-port antenna module and its capability to be closely spaced to adjacent modules lead to a compact size of the 16-port module array or 16 MIMO antennas. In addition, with a low profile and compact size, each antenna in the MIMO array operates in a fractional bandwidth of about 18% (7.025-8.4 GHz) and has port isolation of larger than 10 dB to its nearby antennas.

In the following sections, we present the configurations and design considerations of the low-profile four-port MIMO antenna module and the 16-port closely-spaced 2 × 2 module array. The module array is also fabricated and experimentally studied. The 16 × 8 MIMO system is then tested in our MIMO system testbed [16], [17] by applying the fabricated module array as 16 receive antennas for receiving 8 spatial streams in the 7.1 GHz band (7.025-7.125 GHz). We obtain a spectral efficiency of larger than 56 bps/Hz for the 16 × 8 MIMO system supporting 1024 QAM (10 bits per symbol). The obtained spectral efficiency is larger than three times that (about 16 bps/Hz [13]) of the 5G 4 × 4 MIMO operation in the 3.5 GHz band and is also much larger than that

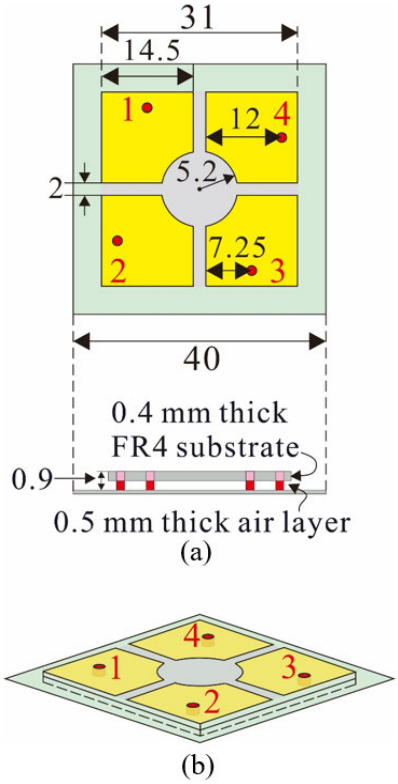

FIGURE 1. Geometry of the low-profile four-port MIMO (4PM) antenna module. (a) Top and side views. (b) Perspective view.

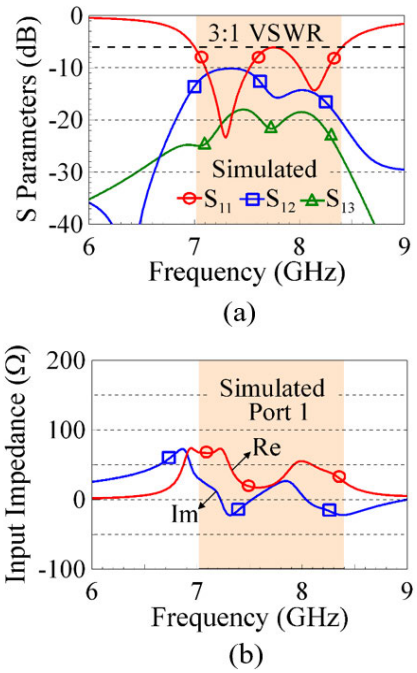

FIGURE 2. Simulated (a) *S* parameters and (b) input impedance of Port 1 in the 4PM antenna module.

(about 34 bps/Hz [9]) of the 8 × 8 MIMO operation in the 7.1 GHz band. Thus, with the proposed module array for the 6G mobile device, the 16 × 8 MIMO system in the upper mid-band will be promising.

II. THE LOW-PROFILE FOUR-PORT MIMO ANTENNA MODULE

Fig. 1 shows the geometry of the low-profile four-port MIMO (4PM) antenna module capable of generating four uncorrelated waves over an operating band of 7.025-8.4 GHz. The 4PM antenna module consists of a square top patch printed on a 0.4 mm thick FR4 substrate (relative permittivity 4.4, loss tangent 0.024), which is spaced by an air layer of thickness 0.5 mm to a ground plane of 40 mm × 40 mm. The total height of the 4PM antenna module is therefore only 0.9 mm (about 0.021λ with respect to the lower-edge frequency 7.025 GHz in the operating band).

The low profile of 0.9 mm allows the antenna module to be allocated in the narrow backcover region of the modern smartphone. In this case, the antenna module does not need to directly occupy any space on the chassis ground of the smartphone. Additionally, owing to the back ground plane of the 4PM antenna module, the effects on the four antennas in the module caused by nearby battery/electronic modules in the smartphone are expected to be small [9], [11].

Also note that the FR4-air layer substrate between the top patch and ground plane of the antenna module has an effective relative permittivity of about 1.52. Although the lower relative permittivity will increase the required patch size for the desired operating band, the four antennas in the antenna module with a low profile of 0.9 mm can have a lower quality factor so as to achieve a wider operating band [18]. In this case, even with a lower relative permittivity, the required top patch size (31 mm × 31 mm) for four antennas is only about 0.73λ × 0.73λ at 7.025 GHz (the lower-edge frequency which generally dominates the antenna size).

To generate four uncorrelated waves, the top patch is separated into four square sub-patches (14.5 mm × 14.5 mm) spaced by 2 mm only to accommodate four ports (Ports 1-4 in Fig. 1). That is, four generally isolated microstrip patch antennas [19] with four sub-patches as their respective radiating patches are formed in the 4PM antenna module. Each port is placed along one centerline of its corresponding sub-patch with a feed position 12 mm to the edge orthogonal to the centerline. Ports 1-4 are then sequentially rotated by 90 degrees [13], [20] to achieve enhanced port isolation of two adjacent sub-patches or two adjacent microstrip patch antennas.

In addition, the inner corners of the four sub-patches are curvedly truncated with a radius of 5.2 mm with respect to the center of the 4PM antenna module. In this case, each microstrip patch antenna can generate two half-wavelength resonant modes (the fundamental resonant modes of microstrip patch antennas [19]) resonated mainly along two orthogonal diagonal lines thereof at close frequencies.

Additionally, the two resonant modes can be excited with good impedance matching and formed together to achieve a wider operating band for each port. Acceptable

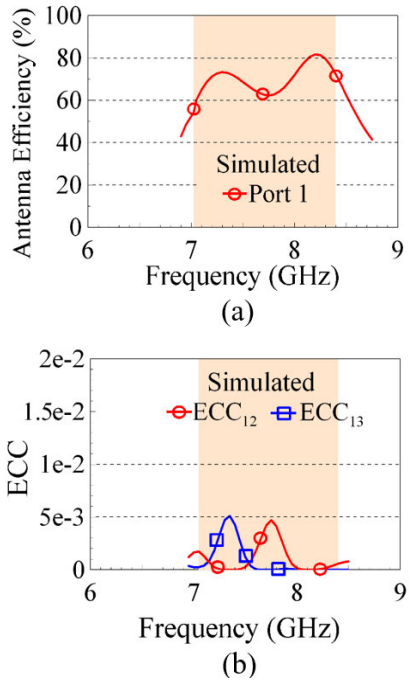

FIGURE 3. Simulated (a) antenna efficiency of Port 1 and (b) envelope correlation coefficients (ECCs) of Ports 1, 2 (two adjacent ports) and Ports 1, 3 (two opposite ports).

port isolation between any two ports is also obtained. Furthermore, with Ports 1-4 rotated by 90 degrees in the four sub-patches, it helps to achieve lower envelope correlation coefficients (ECCs) for the four generated waves, which will be discussed later with the aid of the obtained ECCs in Fig. 3(b).

By using the High Frequency Electromagnetic Simulation Software (ANSYS HFSS) [21], the simulated results of the proposed 4PM antenna module are analyzed. Fig. 2(a) shows the simulated S parameters of Port 1 excited with others terminated to 50 Ω. Two resonant modes excited at about 7.3 and 8.3 GHz are observed. The corresponding input impedance of Port 1 also indicates that two resonances occur at about 7.3 and 8.3 GHz [see Fig. 2(b)].

The colored frequency region in the figure is the desired operating band of 7.025-8.4 GHz. The impedance matching of the two resonant modes over the operating band is better than −6 dB or 3:1 VSWR, which is a widely used criterion for mobile antennas [9], [10], [11], [12], [13], [14], [15], [18], [22]. The transmission coefficient S_{12} (= S_{14}) for two nearby ports is lower than −10 dB, which is acceptable for MIMO mobile antenna applications [9], [10], [11], [12], [13], [14], [15]. The S_{13} for two opposite ports is even lower than −17 dB. Also note that owing to the symmetric structure of the proposed 4PM antenna module, the results of Ports 2-4 are same as that obtained for Port 1.

The simulated antenna efficiency of Port 1 is shown in Fig. 3(a), while the ECCs of Ports 1, 2 (two adjacent ports) and Ports 1, 3 (two opposite ports) obtained based on the far-field radiation patterns [9], [23] are presented in Fig. 3(b). Note that the antenna efficiency is also affected by the

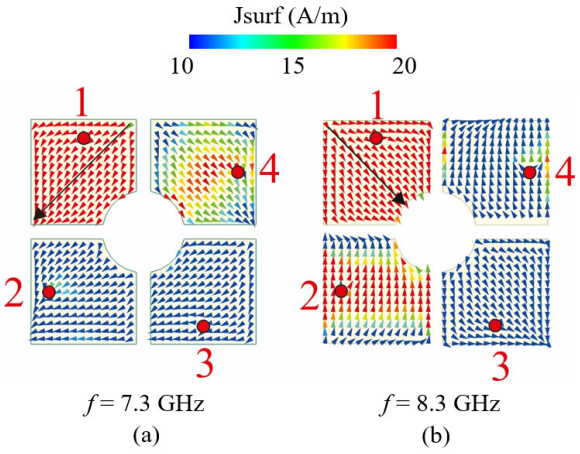

FIGURE 4. Simulated vector surface current distributions in the top patch of the 4PM antenna module; Port 1 is excited with Ports 2-4 terminated to 50 Ω. (a) 7.3 GHz. (b) 8.3 GHz.

coupling of Ports 1-4. The coupling will cause a decrease in the antenna efficiency. With acceptable port isolation or transmission coefficients obtained in the proposed design, the antenna efficiency including the mismatching loss is larger than 56% over the operating band.

For the ECCs of Ports 1, 3 (ECC_{13}) and Ports 1, 2 or 1, 4 ($ECC_{12} = ECC_{14}$), they are all lower than about 0.005. Since the obtained ECCs for any two ports are less than 0.1 [9], [12], the four generated waves of Ports 1-4 in the 4PM antenna module can be considered to be uncorrelated. The four uncorrelated waves will thus be promising to obtain good performance in the MIMO system.

To further verify the excited resonant modes of each port, Fig. 4 shows the simulated vector surface current distributions in the top patch of the 4PM antenna module. The results for Port 1 excited with Ports 2-4 terminated to 50 Ω are shown. The two resonant modes at 7.3 and 8.3 GHz are seen to be in orthogonal polarizations mainly along two diagonal planes [see Fig. 4(a) vs. Fig. 4(b)]. This can be seen more clearly from the corresponding simulated electric field distributions at 7.3 and 8.3 GHz in the median plane (0.45 mm above the ground plane) of the FR4-air layer substrate between the top patch and ground plane (see Fig. 5).

It is seen in Fig. 5 that the two resonant modes have a null electric field in the plane along the diagonal line of their corresponding sub-patch and can both be identified to be half-wavelength resonant modes. In addition, owing to the curvedly truncated inner corner of each sub-patch, the two resonant modes have slightly different resonant lengths. This makes the two resonant modes excited at close frequencies to form a wide operating band.

Fig. 6 shows the corresponding simulated radiation patterns of Port 1 along two principal planes (x-z and y-z planes) at 7.3 and 8.3 GHz. The radiation patterns in two principal planes at 8.3 GHz are seen to be more symmetric than those at 7.3 GHz. This is largely because the resonant mode at 8.3 GHz is resonated along the diagonal

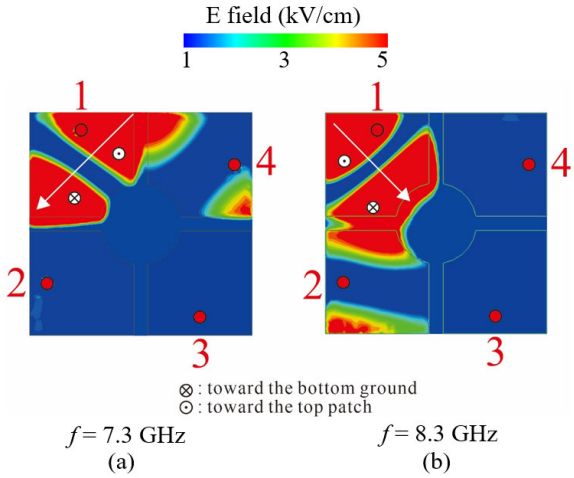

FIGURE 5. Simulated electric field distributions in the median plane between the top patch and ground plane. (a) 7.3 GHz. (b) 8.3 GHz.

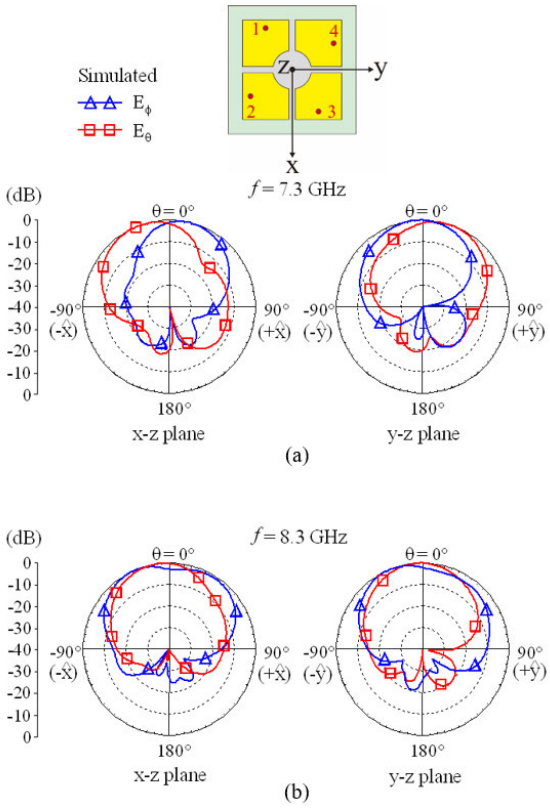

FIGURE 6. Simulated radiation patterns of Port 1. (a) 7.3 GHz. (b) 8.3 GHz.

line toward the curvedly truncated corner, thereby causing generally symmetric excited surface currents with respect to the resonant direction on the sub-patch of Port 1.

Also, for Port 1 excited at 8.3 GHz, it is interesting to observe that, the E_φ pattern appears to be concave in the $\theta = 0^o$ direction in both the *x*-*z* and *y*-*z* planes. This is largely related to the relatively stronger surface currents in the sub-patch with Port 2 than the sub-patch with Port 4 [see Fig. 4(b)]. Both nearby sub-patches with Ports 2 and 4 are respectively coupled through a 2 mm gap to the sub-patch

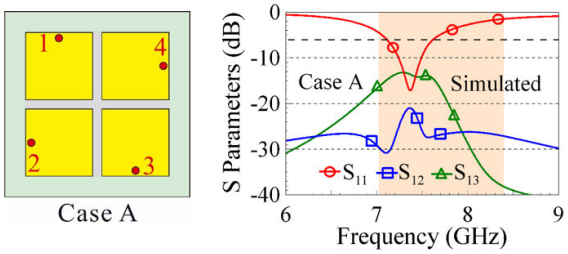

FIGURE 7. Simulated S parameters of Port 1 in Case A for the 4PM antenna module with four simple square sub-patches (no curvedly truncated inner corners for the four sub-patches).

with Port 1. This behavior is probably because Ports 1-4 are not located along the diagonal line of each sub-patch. Thus, with stronger surface currents in the sub-patch with Port 2, it causes the E_φ pattern slightly distorted and its maximum radiation shifted toward the $-x$ direction in the *x*-*z* plane and also toward the $-y$ direction in the *y*-*z* plane. This makes the E_φ pattern to look like concave in the $\theta = 0^o$ direction as seen in Fig. 6(b).

On the other hand, the resonant mode at 7.3 GHz resonates along the diagonal line roughly parallel to the curvedly truncated corner, thus causing asymmetric surface currents with respect to the resonant direction on the sub-patch of Port 1. The radiation patterns in the *x*-*z* and *y*-*z* planes thus tend to be asymmetric at 7.3 GHz.

To address the design considerations of the 4PM antenna module, Fig. 7 shows the simulated *S* parameters of Port 1 in Case A for the antenna module with four simple square sub-patches (that is, no inner curvedly truncated corners for the four sub-patches). The structure of Case A is also shown in the figure. Its corresponding dimensions are same as given in Fig. 1 for the proposed 4PM antenna module.

For Case A, it is seen that only the resonant mode at about 7.3 GHz is excited with good impedance matching, which leads to a narrow bandwidth for the 4PM antenna module. While for the proposed 4PM antenna module, owing to the curvedly truncated inner corners, an additional resonant mode at about 8.3 GHz is excited, which combines with the resonant mode at about 7.3 GHz to form a wider operating band [see Fig. 2(a)].

The corresponding simulated ECCs of Ports 1-4 in Case A are shown in Fig. 8. The ECCs of two opposite ports (ECC_{13}) for Case A reach about 0.18, which is much larger than that (less than about 0.005) for the proposed antenna module [see Fig. 3(b)]. The much larger ECC of Ports 1 and 3 (or Ports 2 and 4) excited at 7.3 GHz is owing to their parallel resonant directions.

On the other hand, the ECC of two nearby ports (Ports 1 and 2 or Ports 1 and 4) is still very low (much less than 0.01). This is related to their orthogonal resonant directions for two nearby ports excited at 7.3 GHz. Owing to the curvedly truncated inner corners of the four sub-patches for bandwidth enhancement in the proposed 4PM antenna module, the ECCs of two nearby ports can also be greatly decreased, making all the ECCs of Ports 1-4 to be less than 0.005 [see Fig. 3(b)].

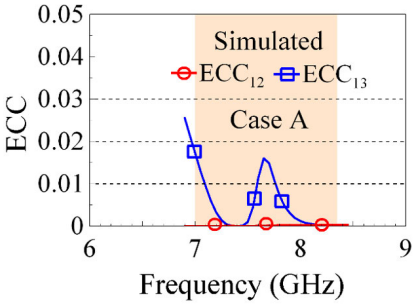

FIGURE 8. Simulated ECCs of ports 1-4 in Case A.

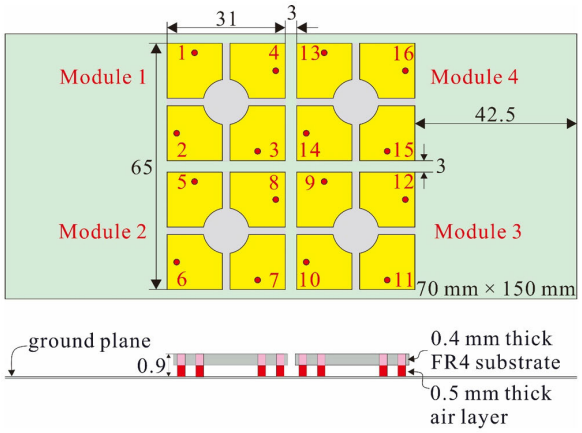

FIGURE 9. Geometry of the 16-port (Ports 1-16) closely-spaced 2 × 2 module array based on using four 4PM antenna modules (Modules 1-4) in Fig. 1. The ground plane of 70 mm × 150 mm for a typical smartphone size is used.

III. THE 16-PORT CLOSELY-SPACED 2 × 2 MODULE ARRAY

By using four 4PM antenna modules (Modules 1-4) of same dimensions as given in Fig. 1 to be closely spaced into a 16-port (Ports 1-16) 2 × 2 module array (see Fig. 9), 16 uncorrelated waves generated by 16 MIMO antennas in a compact structure are obtained. Notice that the spacing of two adjacent modules in the module array is 3 mm only. The 2 × 2 module array hence has a compact size of 65 mm × 65 mm (about 1.5λ × 1.5λ at 7.025 GHz) and can fit in a ground plane of 70 mm × 150 mm, which is a typical modern smartphone size. In addition, with a very low profile of 0.9 mm, it is promising to embed the 2 × 2 module array within the narrow backcover region of the modern smartphone.

Fig. 10 shows the simulated S parameters of the 2 × 2 module array. The S_{11}, S_{12}, S_{13}, and S_{14} for Module 1 are presented in Fig. 10(a). Similar results for Module 1 as in Fig. 2(a) for one antenna module standalone are observed. This indicates that, with a small spacing between the four modules, the S parameters of four antennas in each module are very slightly affected. Fig. 10(b) also shows the S_{22}, S_{23}, S_{25}, S_{28} for Ports 2, 3 in Module 1 and Ports 5, 8 in Module 2. The results for the four innermost ports (Ports 3, 8, 9, 14) in the 2 × 2 array are shown in Fig. 10(c).

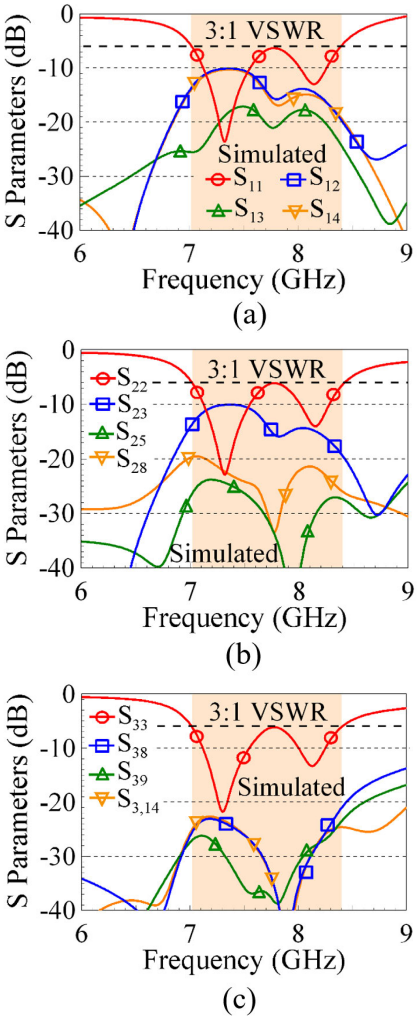

FIGURE 10. Simulated S parameters of the 2 × 2 module array. (a) The S_{11}, S_{12}, S_{13}, S_{14} for Module 1. (b) The S_{22}, S_{23}, S_{25}, S_{28} for Ports 2, 3 in Module 1 and Ports 5, 8 in Module 2. (c) The S_{33}, S_{38}, S_{39}, $S_{3,14}$ for Ports 3, 8, 9, 14 (four innermost ports in the array).

It is interesting to note that the S_{25}, S_{28} in Fig. 10(b) and the S_{38}, S_{39}, and $S_{3,14}$ in Fig. 10(c) for two ports in adjacent modules are less than about −20 dB, which are much lower than the corresponding transmission coefficients between two ports inside each module shown in Fig. 10(a). The enhanced port isolation is largely owing to the air gap (3 mm spacing) between two adjacent modules in the 2 × 2 array (see the side view in Fig. 9). On the other hand, the four sub-patches inside each module are printed on a same 0.4-mm thick FR4 substrate, which may lead to enhanced coupling between adjacent ports, thus having relatively lower port isolation.

Fig. 11(a) shows the simulated antenna efficiency of Ports 1-4 in Module 1. Again, the antenna efficiency is similar to that shown in Fig. 3(a), indicating small effects of nearby modules (Modules 2-4) on Module 1. In addition, the ECCs of the four innermost ports in the 2 × 2 array are also seen to be less than 0.0001 [see Fig. 11(b)]. This further indicates that the proposed 4PM antenna module can be applied to form a closely spaced module array to provide a large number of

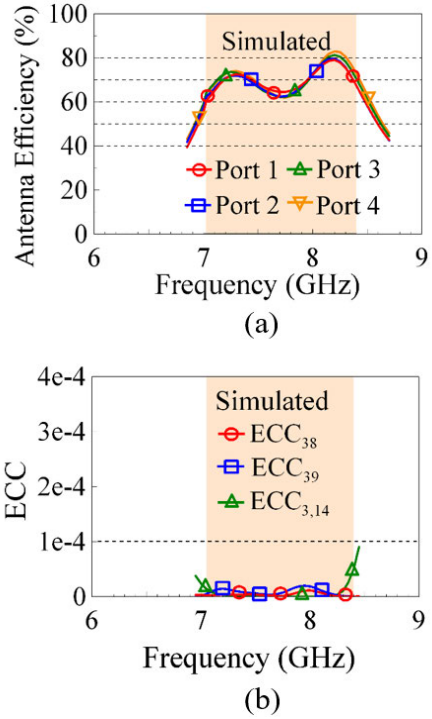

FIGURE 11. Simulated (a) antenna efficiency of Ports 1-4 and (b) envelope correlation coefficients of Ports 3, 8, 9, 14 (four innermost ports in the array).

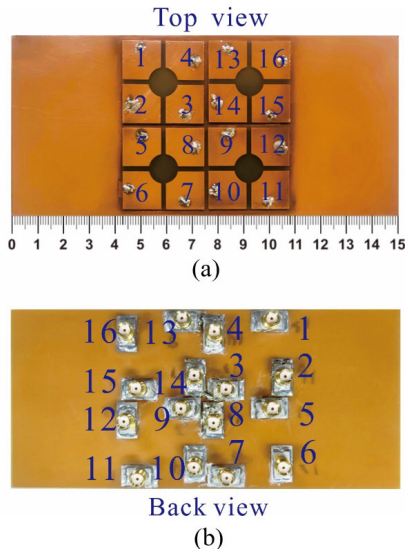

FIGURE 12. Photos of the fabricated 2 × 2 module array. (a) Top view. (b) back view.

MIMO antennas in a compact structure for the 6G mobile device application.

IV. EXPERIMENTAL RESULTS OF THE 2 × 2 MODULE ARRAY

The 2 × 2 module array with 16 MIMO antennas respectively excited by Ports 1-16 was fabricated. Fig. 12 shows the photos of the fabricated module array. The measured reflection coefficients of Ports 1-12 are presented in Fig. 13(a)-(d). The measured results generally match the corresponding

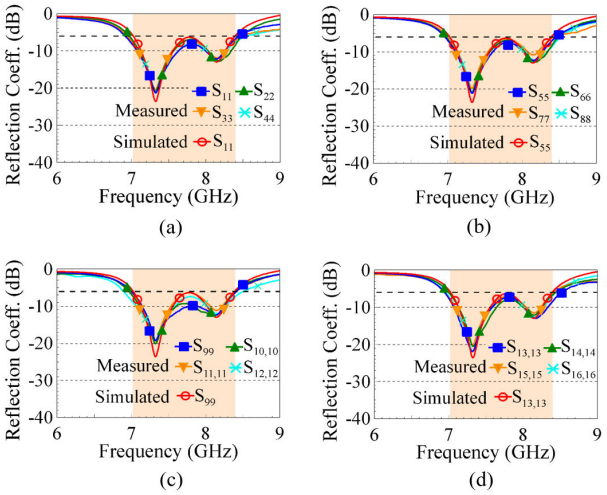

FIGURE 13. Measured reflection coefficients. (a) Ports 1-4. (b) Ports 5-8. (c) Ports 9-12. (d) Ports 13-16.

simulated ones which are also shown in the figure for comparison. Over the desired 7.025-8.4 GHz (the colored frequency region in the figure), each port generates two resonant modes at about 7.3 and 8.3 GHz with good impedance matching less than −6 dB (3:1 VSWR), which meets the widely used criterion for mobile antennas [9], [10], [11], [12], [13], [14], [15], [18], [22].

Fig. 14(a)-(c) shows the measured transmission coefficients. For Port 1 to Ports 2-4 in Module 1, the S_{12} and S_{14} for two adjacent ports are less than -10 dB, while the S_{13} for two opposite ports is less than −17 dB [see Fig. 14(a)]. The measured results are similar to the simulated ones shown in Fig. 2(a) for the 4PM antenna module standalone. The measurement confirms that although there are three adjacent modules, the transmission coefficients of Ports 1-4 in Module 1 are slightly affected.

For Port 2 to Port 3 in Module 1 and to nearby Ports 5, 8 in Module 2, the measured transmission coefficients also agree with the simulated ones [see Fig. 14(b) vs. Fig. 10(b)].

The measured transmission coefficients of the four innermost ports (Ports 3, 8, 9, 14) in the 2 × 2 module array are less than −20 dB [see Fig. 14(c)]. The results are in agreement with the simulated ones in Fig. 10(c). The port isolation larger than 20 dB for two ports in adjacent modules may be related to the low profile (0.9 mm) of the modules and the 3 mm air gap between adjacent modules in the array.

Note that the air gap spacing is larger than three times that of the module height or the antenna height. Owing to the antenna's low profile, the fringing fields at the patch edges of the four antennas in each 4PM antenna module excited in their fundamental half-wavelength resonant modes will travel in a relatively short distance away from the patch edges.

Therefore, with the air gap between adjacent modules selected to be larger than three times the antenna height in this study, enhanced port isolation for two ports in adjacent modules is obtained. This can provide as a design guide

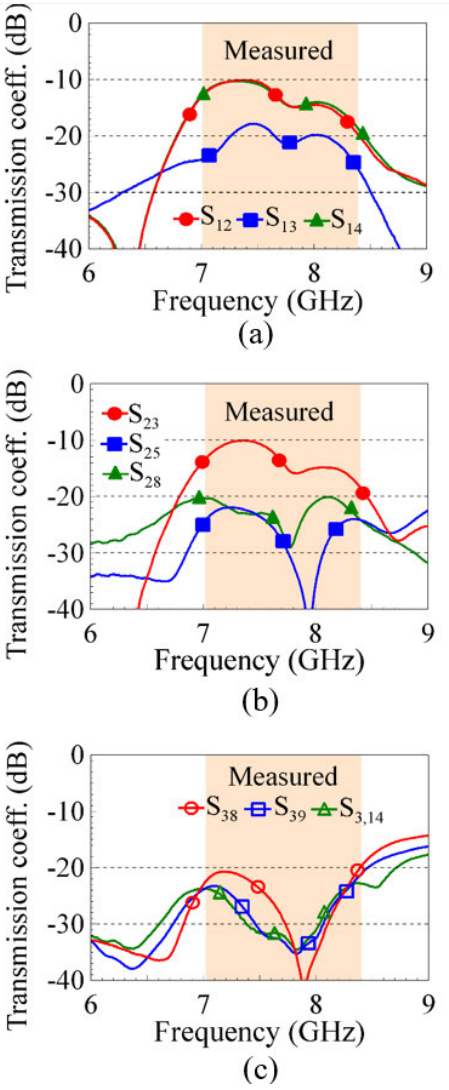

FIGURE 14. Measured transmission coefficients. (a) Port 1 to Ports 2-4 in Module 1. (b) Port 2 to Port 3 in Module 1 and to nearby Ports 5, 8 in Module 2. (c) Ports 3, 8, 9, 14 of the four innermost ports in the module array.

for selecting a proper spacing between the modules in the proposed 2 × 2 module array. Similar measured transmission coefficients of Ports 9-12 in Module 3 and Ports 13-16 in Module 4 have also been obtained. For brevity, these measured results are not presented.

The fabricated 2 × 2 module array is further tested in the far-field anechoic chamber to evaluate its radiation characteristics. Fig. 15 shows the experimental setup in the far-field anechoic chamber. Fig. 16 shows the measured antenna efficiency obtained based on applying the Great Circle Test method for mobile terminals [24], in which the module array is rotated in both the azimuthal and roll directions to obtain the total radiated power for each port. The antenna efficiency is then evaluated.

The results for the 16 MIMO antennas with Ports 1-16 are respectively shown in Fig. 16(a)-(d). The measured antenna efficiency for each port is better than 55% in the operating

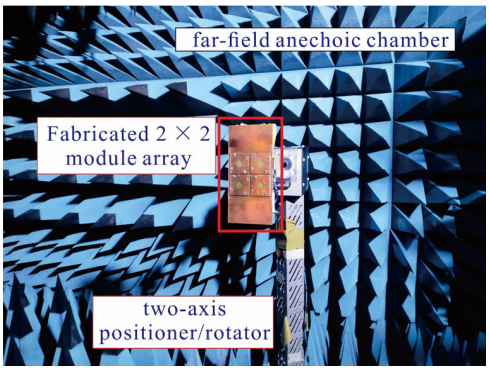

FIGURE 15. Experimental setup of the fabricated 2 × 2 module array in the far-field anechoic chamber.

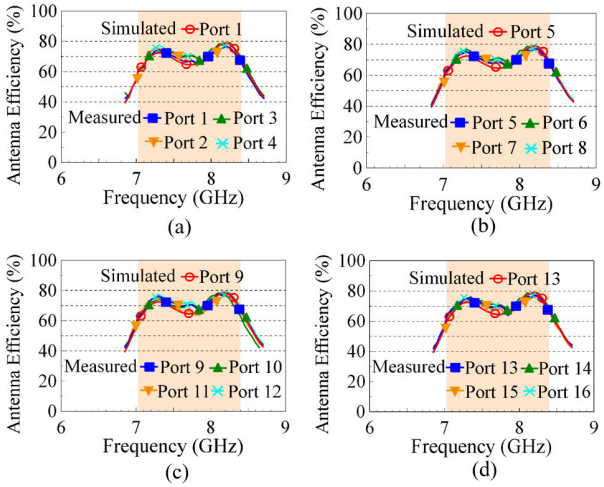

FIGURE 16. Measured antenna efficiency. (a) Ports 1-4. (b) Ports 5-8. (c) Ports 9-12. (d) Ports 13-16.

band of 7.025-8.4 GHz. The results also generally match the simulated ones in Fig. 11(a).

Fig. 17 shows the calculated ECCs using the measured electric fields of the three-dimensional radiation patterns [9], [23]. Representative results of the four ports in Module 1 [see Fig. 17(a)] and the four innermost ports in the module array [see Fig. 17(b)] are presented. For Ports 1-4 in Module 1, the ECC_{mn} of Ports m and n are less than 0.006. On the other hand, the ECC_{mn} of two ports in the four innermost ports (Ports 3, 8, 9, 14) in the module array is even less than 0.0001.

The obtained ECC values fairly agree with the simulated results shown in Figs. 3(b) for the 4PM antenna module standalone (ECCs less than 0.005) and Fig. 11(b) for the four innermost ports in the module array (ECCs less than 0.0001). In this case, with the obtained ECCs less than 0.1 [9], [12], the 16 waves generated by the 16 MIMO antennas in the module array are considered to be uncorrelated. That is, the 16 MIMO antennas will be promising for practical MIMO applications.

Representative measured radiation patterns for Ports 1 and 3 in Module 1 of the 2 × 2 module array are also plotted in Fig. 18. The radiation patterns in two principal planes (x-z and y-z planes) are normalized with respect to the same maximum value. The results at 7.3 GHz and 8.3 GHz for the

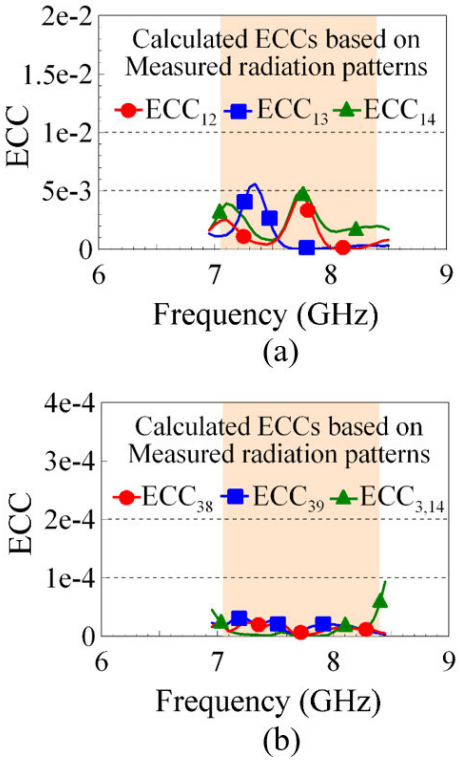

FIGURE 17. Calculated ECCs using the measured electric fields of the three-dimensional radiation patterns. (a) The ECC_{mn} of Ports m and n in Module 1. (b) The ECC_{mn} of two ports in the four innermost ports (Ports 3, 8, 9, 14) in the module array.

two half-wavelength resonant modes excited in orthogonal planes for each port are shown.

The corresponding simulated results are also plotted in the figure for comparison. The measured radiation patterns generally agree with the simulated ones. More symmetric radiation patterns at 8.3 GHz than those at 7.3 GHz are observed. This behavior is mainly caused by the curvedly truncated inner corners for each sub-patch in the 4PM antenna module. The truncated inner corner leads to some asymmetric surface current distribution at 7.3 GHz, with relatively very small effects on the surface current distribution at 8.3 GHz.

The measured antenna gains for Ports 1 and 3 are respectively about 8.55 dBi and 8.48 dBi at 7.3 GHz, while those for Ports 1 and 3 are respectively 7.44 dBi and 7.35 dBi at 8.3 GHz. The measured antenna gains are indicated in Fig. 18. The measured maximum radiation direction and half-power beamwidth in the *x*-*z* and *y*-*z* planes of Ports 1 and 3 are also listed in Table 1 for comparison.

The radiation patterns for the remaining ports in the fabricated module array have also been measured. Similar charactreisics as discussed for those of Ports 1 and 3 shown in Fig. 18 are observed. For brevity, the measured radiation patterns of the remaining ports are not presented. Based on the obtained results in this section, it indicates that the fabricated 2 × 2 module array can provide 16 MIMO antennas with acceptable impedance matching, port isolation, and low ECC charactreistics for the proposed 16 × 8 MIMO operation.

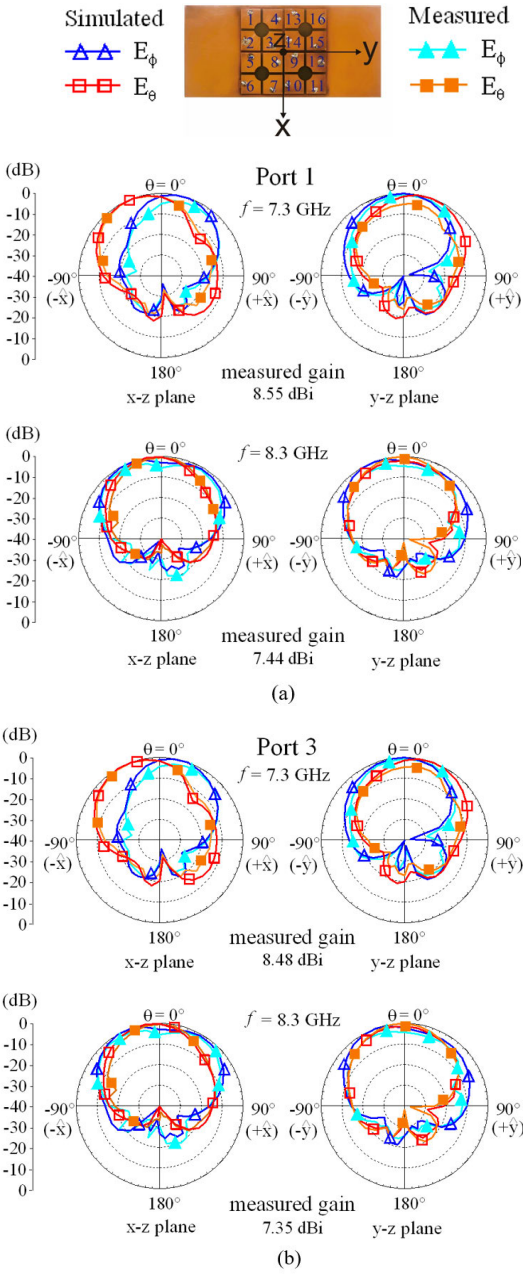

FIGURE 18. Measured and simulated normalized radiation patterns for representative ports in Module 1 at 7.3 GHz and 8.3 GHz. (a) Port 1. (b) Port 3.

V. 16 × 8 MIMO SYSTEM TESTING OF THE FABRICATED 2 × 2 MODULE ARRAY

The fabricated 2 × 2 module array with 16 MIMO antennas is applied as 16 receive (Rx) antennas in the 16 × 8 MIMO system to evaluate its MIMO performance. Fig. 19 shows the 16 × 8 MIMO testbed at National Sun Yat-sen University (NSYSU) [9], [12], [16], [17]. The 8-port MIMO patch antenna provides 8 transmit (Tx) antennas [25] at the transmitter to transmit 8 spatial streams in the 16 × 8 MIMO system. Ports 1-16 of the fabricated 2 × 2 module array are used to receive the 8 spatial streams and are connected to four high-performance four-port digital oscilloscopes. The

TABLE 1. Measured maximum radiation direction and half-power beamwidth of Ports 1 and 3 in Fig. 18. For the *x-z* plane, the positive (negative) radiation direction to 6 = 0° (the *z* axis) indicates toward the +*x* (-x) direction. For the *y-z* plane, the positive (negative) radiation direction to 0 = 0° indicates toward the + *y (-y)* direction.

	Maximum Radiation Direction		Half-Power Beamwidth	
Port 1 [Fig. 18(a)]	*x-z* plane	*y-z* plane	*x-z* plane	*y-z* plane
E_ϕ pattern at 7.3 GHz	+10° to θ = 0°	-5° to θ = 0°	55°	54°
E_θ pattern at 7.3 GHz	-20° to θ = 0°	+10° to θ = 0°	50°	53°
E_ϕ pattern at 8.3 GHz	-30° to θ = 0°	-30° to θ = 0°	50°	80°
E_θ pattern at 8.3 GHz	-5° to θ = 0°	at θ = 0°	55°	65°
Port 3 [Fig. 18(b)]	*x-z* plane	*y-z* plane	*x-z* plane	*y-z* plane
E_ϕ pattern at 7.3 GHz	+20° to θ = 0°	-5° to θ = 0°	57°	60°
E_θ pattern at 7.3 GHz	-20° to θ = 0°	+10° to θ = 0°	60°	56°
E_ϕ pattern at 8.3 GHz	-30° to θ = 0°	-30° to θ = 0°	50°	90°
E_θ pattern at 8.3 GHz	-5° to θ = 0°	at θ = 0°	55°	65°

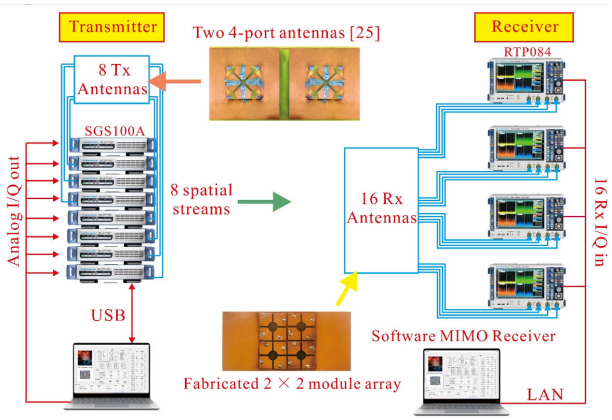

FIGURE 19. The 16 × 8 MIMO system testbed at National Sun Yat-sen University (NSYSU). The fabricated module array with 16 ports is applied as the 16 receive (Rx) antennas. The 8-port MIMO patch antenna [25] is used as the 8 transmit (Tx) antennas at the transmitter.

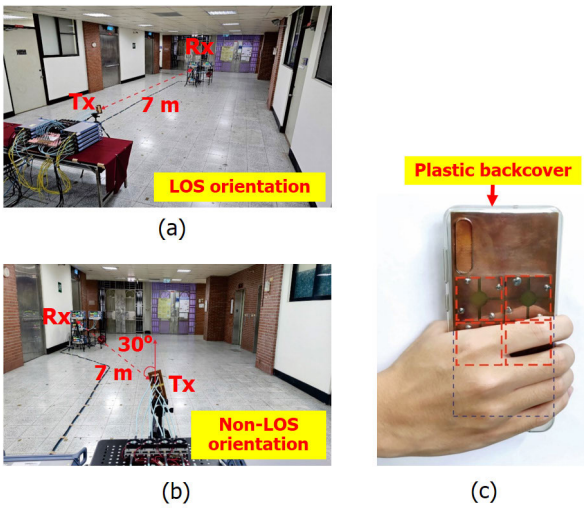

FIGURE 20. The 16 × 8 MIMO system testing with the open indoor scenario inside the electrical engineering department building, NSYSU. (a) Tx and Rx antennas with LOS orientation. (b) Tx antennas fixed and Rx antennas moved 30 degrees away from the LOS orientation. (c) The case of user's hand (one of the authors) holding the fabricated module array, which is placed behind a plastic backcover in the testing.

16 received signals are then fed into a software MIMO receiver to retrieve the original data transmitted through 8 spatial streams.

Fig. 20(a) and (b) show the 16 × 8 MIMO system testing scenario (LOS in an open wide corridor inside the electrical engineering department building at National Sun Yat-sen University (NSYSU)). The wide corridor measuring 19 meters by 6.6 meters is adjacent to an elevator of the department building and is open to the public. That is, the 16 × 8 MIMO testing is conducted in a practical indoor public area. The distance between the 8 Tx antennas at the transmitter and the 16 Rx antennas at the receiver is 7 meters.

Notice that the 16 Rx antennas provided by the fabricated 2 × 2 module array are mounted on a ground plane of size 150 mm × 70 mm to simulate that the module array is applied in the backcover region of the modern smartphone [9]. Two use cases of the 16 Rx antennas standalone (Case SA) and with the user's hand holding (Case HH) [see Fig. 20(c)] are tested. For the hand holding case, about 8 Rx antennas or one half of the 16 Rx antennas are covered by the user's hand. Also note that for Case HH, one of the authors acting as the user holds the fabricated module array and stands alongside the Rx side in the testing.

Additionally, for each use case, the LOS [the Rx antennas facing the Tx antennas in the line-of-sight (LOS) orientation as seen in Fig. 20(a)] and the NLOS [Non-LOS, the Rx antennas moved 30 degrees away from the LOS orientation with the Tx antennas fixed as seen in Fig. 20(b)] are tested. That is, four cases of SA-LOS, HH-LOS, SA-NLOS, and HH-NLOS are tested for the 16 × 8 MIMO system in a practical open indoor scenario.

The measured results of the 16 × 8 MIMO system are given in Table 2. The frequency band of 7.025-7.125 GHz

TABLE 2. Measured results of the 16 x 8 MIMO system using the fabricated 16-port 2 × 2 module array as 16 receive (Rx) antennas in the 7.1 GHz band (7.025-7.125 GHz); At the transmitter, two 4-port MIMO patch antennas [25] are used as 8 transmit (Tx) antennas for 8 spatial streams. The Rx antennas in both the standalone (SA) and the user's hand holding (HH) conditions are tested. The NLOS (non-LOS) orientation is the Rx antennas moved 30 degrees away from the LOS (line-of-sight) orientation with the Tx antennas fixed.

f_0 = 7.075 GHz (7.025-7.125 MHz), 16 × 8 MIMO, Open indoor Scenario, Distance between Tx and Rx = 7 m				
Rx-Tx Orientation	LOS (Line-of-Sight)		NLOS (Non-Line-of-Sight)	
Standalone (SA) or User's Hand Holding (HH)	SA-LOS case	HH-LOS case	SA-NLOS case	HH-NLOS case
Signal Modulation	1024 QAM	1024 QAM	1024 QAM	256 QAM
Measured Signal Noise Ratio (dB) of 16 Ports in the 2 x 2 module array (Rx antennas)	29.9, 27.7, 30.2, 28.6 28.3, 29.4, 28.3, 28.7 27.8, 29.1, 29.0, 28.1 29.0, 29.1, 29.3, 30.3 (Ports 1-16 at Rx, Ave. SNR ≈ 29.0 dB)	29.1, 27.6, 30.1, 28.8 28.1, 28.3, 28.1, 28.3 28.4, 25.4, 27.0, 24.4 20.3, 25.0, 21.1, 23.1 (Ports 1-16 at Rx, Ave. SNR ≈ 27.2 dB)	30.1, 28.4, 28.1, 29.0 28.8, 31.0, 29.0, 28.7 28.8, 30.8, 28.3, 30.0 29.8, 28.5, 29.9, 28.6 (Ports 1-16 at Rx, Ave. SNR ≈ 29.3 dB)	29.1, 28.2, 29.5, 28.9 28.4, 28.0, 25.9, 27.3 22.6, 20.9, 20.8, 22.9 15.4, 14.6, 10.9, 20.1 (Ports 1-16 at Rx, Ave. SNR ≈ 26.0 dB)
Calculated MIMO Capacity (A) (Assuming rich scattering)	82.2 bps/Hz	76.9 bps/Hz	82.9 bps/Hz	72.5 bps/Hz
Measured MIMO Capacity (B)	74.3 bps/Hz	67.6 bps/Hz	72.3 bps/Hz	59.6 bps/Hz
MIMO Efficiency (B/A)	90.4%	87.9%	87.2%	82.2%
Uncoded Bit Error Rate	0.021	0.043	0.037	0.027
Coded Bit Error Rate	0	0	0	0
Measured Throughput	5745 Mbps	5618 Mbps	5659 Mbps	4570 Mbps
Spectral Efficiency	57.45 bps/Hz	56.18 bps/Hz	56.59 bps/Hz	45.70 bps/Hz

(100 MHz bandwidth) is tested, which is a promising new international mobile telecommunication (IMT) band for the global regions and is expected to be identified in World Radiocommunication Conference 2023 (WRC-23) [7]. For each case in the MIMO testing, the signal modulation that can be supported is given in the table. The two standalone cases (SA-LOS, SA-NLOS) and even the hand holding case with the LOS orientation (HH-LOS) can support up to the 1024 QAM signal modulation. For the hand holding case with the non-LOS orientation (HH-NLOS), the 256 QAM signal modulation can be supported. The measured signal noise ratios (SNRs) of the 16 antennas in the fabricated 2 × 2 module array are recorded.

Owing to the hand holding which covers about one half of the 16 Receive antennas, the average SNRs for the two hand holding cases are about 1.8 dB or 3.3 dB lower than those of the two standalone cases with the LOS (29.0 vs. 27.2 dB) or non-LOS (29.3 vs. 26.0 dB) orientations, respectively. This leads to lower calculated and measured 16 × 8 MIMO capacity for the hand holding cases, as compared to the standalone cases. The different decreases in the average SNRs are owing to slightly different hand holdings in the LOS and non-LOS orientations.

Also note that the calculated MIMO capacity is obtained based on assuming rich scattering in the testing environment. Thus, the calculated MIMO capacity can be considered to be an ideal capacity for the 16 × 8 MIMO system. On the other hand, the measured MIMO capacity is obtained based on the real scattering behavior in the open indoor environment in the testing. Therefore, the ratio of the measured capacity to the calculated one is provided as the MIMO efficiency in the table. For 100% MIMO efficiency, it indicates that the measured capacity is same as the calculated one, and the testing environment can be considered to show an ideally rich scattering property.

In the obtained results, the MIMO efficiency for the four cases is larger than 82%. That of the standalone case with LOS orientation (SA-LOS) is even larger than 90%. This suggests that with the 16 Rx antennas used to receive the 8 spatial streams, good MIMO performance is obtained. This makes the 16 × 8 MIMO system promising to support up to 1024 QAM signal modulation for the standalone cases and at least 256 QAM or even 1024 QAM for the hand holding cases. Larger data throughput and spectral efficiency of the 16 × 8 MIMO system can thus be obtained.

To determine whether the 16 × 8 MIMO system supports the 1024 QAM or 256 QAM signal modulation, the coded bit error rate (BER) should be zero and the uncoded BER is generally less than 0.1 [9]. The uncoded BER is a direct measure of the ratio of the erroneous bits received to the total bits of the original data transmitted in the 16 × 8 MIMO system. When the uncoded BER is lower than 0.1, the received erroneous bits at the receiver can generally be corrected by applying a decoder to obtain a zero coded BER [9].

From the obtained results, the two standalone (SA-LOS, SA-NLOS) cases and even the hand holding case with the LOS orientation (HH-LOS) support the 1024 QAM signal modulation. The measured throughput is larger than 56 bps/Hz, which is the total correct data received at the

receiver and is calculated from the total transmitted data times (1 – measured uncoded BER). The corresponding spectral efficiency obtained from the measured throughput divided by 100 MHz (the operating band in the 16 × 8 MIMO testing) is larger than 56 bps/Hz, which is much larger than that (about 34 bps/Hz) of the 8 × 8 MIMO system supporting 64 QAM only [9].

While for the hand holding case with non-LOS orientation (HH-NLOS), the 16 × 8 MIMO system can support the 256 QAM signal modulation and the measured throughput is larger than 4.5 Gbps. The corresponding spectral efficiency is about 45 bps/Hz. It is also much larger than that (about 34 bps/Hz) of the 8 × 8 MIMO system supporting 64 QAM only, in which only 8 Rx antennas are used in the standalone condition [9]. It should be noted that, for the hand holding case, the 8 × 8 MIMO system is very likely not able to support 64 QAM, which will lead to a lower spectral efficiency that that reported in [9].

VI. CONCLUSION

For the 6G upper mid-band mobile device to operate in a higher-order MIMO system such as the 16 × 8 MIMO system, a 16-port closely-spaced 2 × 2 module array formed by four low-profile four-port MIMO antenna modules covering 7.025-8.4 GHz has been proposed. The 2 × 2 module array shows a compact size to fit in the backcover region of the modern smartphone, making it conveniently to embed a large number of MIMO antennas therein. The design considerations of the proposed 2 × 2 module array have been addressed. The fabricated 2 × 2 module array is also tested as 16 Rx antennas in the 16 × 8 MIMO system in a practical open wide corridor inside the electrical engineering department building at NSYSU. The obtained spectral efficiency is larger than 56 bps/Hz for the tested 16 × 8 MIMO system, which is larger than three times that (about 16 bps/Hz) of the 5G 4 × 4 MIMO operation [13] and is also much larger than that (about 34 bps/Hz) of the 8 × 8 MIMO operation in the 7.1 GHz band [9] (all for the standalone case). The results reveal that, by applying more Rx antennas than the number of spatial streams in the MIMO system, a much larger spectral efficiency can be obtained. That is, the user can experience a much larger data throughput. Based on the obtained results, the proposed closely-spaced module array capable of providing high-density or more MIMO antennas in the limited space inside the modern smartphone will be promising for 6G mobile communication applications featuring 8 spatial MIMO streams.

REFERENCES

[1] (Jan. 7, 2022). *MediaTek 6G Vision Whitepaper*. [Online]. Available: https://www.mediatek.com/whitepapers/6g

[2] Huawei 6G Research Team. (Nov. 1, 2021). *6G: The Next Horizon*. [Online]. Available: https://www.huawei.com/en/technology-insights/future-technologies/6g-the-next-horizon

[3] (Oct. 1, 2021). *Nokia Bell Labs Whitepaper: Extreme Massive MIMO for Macro Cell Capacity Boost in 5G-Advanced and 6G*. [Online]. Available: https://www.bell-labs.com/institute/white-papers/extreme-massive-mimo-for-macro-cell-capacity-boost-in-5g-advanced-and-6g/#gref

[4] (May 1, 2022). *Samsung 6G Whitepaper: Spectrum Expanding the Frontier*. [Online]. Available: https://cdn.codeground.org/nsr/downloads/researchareas/2022May_6G_Spectrum.pdf

[5] J. Rosenworcel. (Mar. 1, 2022). *New Frontiers of Partnerships*. [Online]. Available: https://www.fcc.gov/document/chairwoman-rosenworcel-remarks-mobile-world-congress-2022

[6] K. Lee, J. Kim, E. W. Jin, and K. S. Kim, "Extreme massive MIMO for upper-mid band 6G communications," *Proc. 13th Int. Conf. Inf. Commun. Technol. Converg. (ICTC)*, Jeju Island, South Korea, Oct. 2022, pp. 997–999.

[7] (Nov. 6, 2019). *WRC-19 (World Radiocommunication Conference 2019) Report. Key Outcomes of the WRC-19*. [Online]. Available: https://www.itu.int/en/itunews/Documents/2019/2019-06/2019_ITUNews06-en.pdf

[8] U.S. House of Representatives, Subcommittee on Communications & Technology (Mar. 16, 2022). *CTIA on, 5G and Beyond: Exploring the Next Wireless Frontier*. [Online]. Available: https://docs.house.gov/Committee/Calendar/ByEvent.aspx?EventID114488

[9] K.-L. Wong, H.-C. Kao, and W.-Y. Li, "Wideband low-profile eight-port eight-wave annular-ring patch antenna based on using eight dual-shorted dual-resonant ring sectors for 8 × 8 MIMO mobile devices," *IEEE Access*, vol. 11, pp. 18–32, 2023.

[10] C. Tsai, K. Wong, and W. Li, "Experimental results of the multi-Gbps smartphone with 20 multi-input multi-output (MIMO) antennas in the 20 × 12 MIMO operation," *Microw. Opt. Technol. Lett.*, vol. 60, no. 8, pp. 2001–2010, Aug. 2018.

[11] D. Q. Liu, H. J. Luo, M. Zhang, H. L. Wen, B. Wang, and J. Wang, "An extremely low-profile wideband MIMO antenna for 5G smartphones," *IEEE Trans. Antennas Propag.*, vol. 67, no. 9, pp. 5772–5780, Sep. 2019.

[12] K.-L. Wong, C.-J. Ho, and W.-Y. Li, "Low-profile six-port circular patch antenna with six triple-shorted dual-resonant 60°-disk sectors to generate six uncorrelated waves for wideband mobile MIMO antennas," *IEEE Access*, vol. 10, pp. 80277–80288, 2022.

[13] I. R. R. Barani, K.-L. Wong, Y.-X. Zhang, and W.-Y. Li, "Low-profile wideband conjoined open-slot antennas fed by grounded coplanar waveguides for 4 × 4 5G MIMO operation," *IEEE Trans. Antennas Propag.*, vol. 68, no. 4, pp. 2646–2657, Apr. 2020.

[14] K.-L. Wong, C.-J. Chen, and W.-Y. Li, "Integrated four low-profile shorted patch dual-band WLAN MIMO antennas for mobile device applications," *IEEE Trans. Antennas Propag.*, vol. 69, no. 6, pp. 3566–3571, Jun. 2021.

[15] L. Chang and H. Wang, "Miniaturized wideband four-antenna module based on dual-mode PIFA for 5G 4 × 4 MIMO applications," *IEEE Trans. Antennas Propag.*, vol. 69, no. 9, pp. 5297–5304, Sep. 2021.

[16] K.-L. Wong, "5G/B5G multi-Gbps antennas for user terminals and their throughput verification," in *Proc. IEEE Asia–Pacific Microw. Conf. (APMC)*, Hong Kong, Dec. 2020, pp. 366–368.

[17] K.-L. Wong, Y.-R. Chen, and W.-Y. Li, "Eight-planar-monopole MIMO circular array generating eight uncorrelated waves for 6G upper mid-band 8 × 8 MIMO access points," *IEEE Access*, vol. 11, pp. 68018–68030, 2023.

[18] K.-L. Wong, M.-F. Jian, and W.-Y. Li, "Low-profile wideband four-corner-fed square patch antenna for 5G MIMO mobile antenna application," *IEEE Antennas Wireless Propag. Lett.*, vol. 20, no. 12, pp. 2554–2558, Dec. 2021.

[19] K. L. Wong, *Compact and Broadband Microstrip Antennas*. New York, NY, USA: Wiley, 2002.

[20] K.-L. Wong, S.-W. Su, and Y.-L. Kuo, "A printed ultra-wideband diversity monopole antenna," *Microw. Opt. Technol. Lett.*, vol. 38, no. 4, pp. 257–259, Aug. 2003.

[21] ANSYS HFSS. (Mar. 1, 2022). *3D High Frequency Electromagnetic Simulation Software*. [Online]. Available: https://www.ansys.com/products/electronics/ansys-hfss

[22] Y.-L. Ban, C. Li, C.-Y.-D. Sim, G. Wu, and K.-L. Wong, "4G/5G multiple antennas for future multi-mode smartphone applications," *IEEE Access*, vol. 4, pp. 2981–2988, 2016.

[23] A. Iqbal, A. Altaf, M. Abdullah, M. Alibakhshikenari, E. Limiti, and S. Kim, "Modified U-shaped resonator as decoupling structure in MIMO antenna," *Electronics*, vol. 9, no. 8, p. 1321, Aug. 2020.

[24] Y. Okano and K. Cho, "Antenna measurement system for mobile terminals," *NTT DoCoMo Tech. J.*, vol. 9, no. 2, pp. 43–50, 2007.

[25] K.-L. Wong, X.-Q. Ye, and W.-Y. Li, "Wideband four-port single-patch antenna based on the quasi-$TM_{1/2,1/2}$ mode for 5G MIMO access-point application," *IEEE Access*, vol. 10, pp. 9232–9240, 2022.

KIN-LU WONG (Fellow, IEEE) received the B.S. degree in electrical engineering from the National Taiwan University, Taipei, Taiwan, in 1981, and the M.S. and Ph.D. degrees in electrical engineering from Texas Tech University, Lubbock, TX, USA, in 1984 and 1986, respectively.

From 1986 to 1987, he was a Visiting Scientist with the Max Planck Institute for Plasma Physics, Munich, Germany. Since 1987, he has been with the Electrical Engineering Department, National Sun Yat-sen University (NSYSU), Kaohsiung, Taiwan, where he became a Professor, in 1991. From 1998 to 1999, he was a Visiting Scholar with the Electro Science Laboratory, The Ohio State University, Columbus, OH, USA. He was elected to be a Sun Yat-sen Chair Professor (2005) and a Distinguished Chair Professor (2017) with NSYSU, and the National Chair Professor of the Ministry of Education (MOE) of Taiwan, in 2016. He was also the Chairperson of the Electrical Engineering Department, from 1994 to 1997; the Vice President of Research Affairs, from 2005 to 2007; and the Senior Vice President with NSYSU, from 2007 to 2012. He is currently the Director of the 6G Communication and Sensing Research Center, funded by the Ministry of Education. He has authored more than 580 refereed journal articles and 300 conference papers and has personally supervised 57 graduated Ph.D. He holds over 300 patents, including 105 U.S. patents. He is the author of *Design of Nonplanar Microstrip Antennas and Transmission Lines* (Wiley, 1999), *Compact and Broadband Microstrip Antennas* (Wiley, 2002), and *Planar Antennas for Wireless Communications* (Wiley, 2003). His published articles have been cited over 35,700 times with an H-index of 87 in Google Scholar.

Dr. Wong served as an IEEE AP-S AdCom Member, an IEEE TRANSACTIONS ON ANTENNAS AND PROPAGATION (TAP) Track Editor/an Associate Editor, an IEEE TAP Paper Awards Committee Member, and an AP-Society Field Awards Committee Member. He was a PE7 Panel Member of the European Research Council Advanced Grant Panel, in 2015, 2017, and 2019; and a Chief Consultant of the Institute of Antenna Engineers of Taiwan. He received the Outstanding Research Award from the Taiwan National Science Council, for three times (1995, 2000, and 2002). He also received the Outstanding Electrical Engineering Professor Award from the Institute of Electrical Engineers of Taiwan, in 2003; and the Outstanding Engineering Professor Award from the Institute of Engineers of Taiwan, in 2004. In 2008, the research achievements on handheld device antennas of NSYSU Antenna Laboratory, led by him was selected to be top 50 scientific achievements of the Taiwan Ministry of Science and Technology in past 50 years (1959–2009). He was a recipient of the 2010 Outstanding Research Award of Pan Wen Yuan Foundation and selected as top 100 Honor of Taiwan by Global Views Monthly, in August 2010, for his contribution in mobile antenna researches. He was also a recipient of the Academic Award from the Taiwan Ministry of Education, in 2012, and the Outstanding Distinguished Researcher Award from the Taiwan Ministry of Science and Technology, in 2013. He and his graduate students have received the Best Paper Award (APMC Prize) from 2008 APMC; and the Best Student Paper Award/Young Scientist Award from 2007 ISAP, 2008 APMC, 2009 ISAP, 2010 ISAP, 2012 ISAP, and 2016 ISAP. His graduate students also won the first prize of 2007 and 2009 Taiwan National Mobile Handset Antenna Design Competition. He received the Best Associate Editor for IEEE TRANSACTIONS ON ANTENNAS AND PROPAGATION, for two times (2015 and 2016). He served as the Chair for the Judge Panel of the National Communication Antenna Design Competition, from 2014 to 2023, organized by the Taiwan Ministry of Economics. He also served as the General Chair for 2012 APMC, 2014 ISAP, and 2016 APCAP held at Kaohsiung, and will also serve as the Honorary General Chair for 2023 APMC held at Taipei. He was elected as a Thomson Reuters Highly Cited Researcher, in 2014 and 2015, and also an Elsevier Most Cited Researcher, in 2015. In 2022, he was selected by Research.com to be ranked 99 in Full World Ranking and ranked 1 in Full Taiwan Ranking in the 2022 Edition of Ranking of Top 1000 Scientists in the field of electronics and electrical engineering. He is a Distinguished Researcher of the National Science and Technology Council.

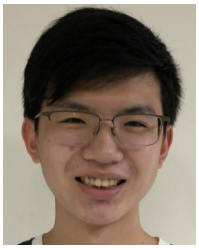

SHAO-EN HONG (Student Member, IEEE) received the B.S. degree in communications engineering from Feng Chia University, Taichung, Taiwan, in 2022. He is currently pursuing the M.S. degree with the National Sun Yat-sen University, Kaohsiung, Taiwan. His main research interests include 6G upper mid-band MIMO antennas for next-generation mobile devices and their MIMO performance evaluation.

WEI-YU LI (Member, IEEE) was born in Taipei, Taiwan, in 1981. He received the B.S. degree in electrical engineering from Feng Chia University, Taichung, Taiwan, in 2004, and the M.S. and Ph.D. degrees in electrical engineering from the National Sun Yat-sen University (NSYSU), Kaohsiung, Taiwan, in 2006 and 2009, respectively.

After graduated from NSYSU, in 2009, he has been with the Information and Communication Research Laboratories (ICL), Industrial Technology Research Institute (ITRI), Hsinchu, Taiwan, participating and leading advanced research for development of emerging wireless antenna technologies. From April 2012 to October 2012, he was an Exchange Guest Researcher with the National Institute of Information and Communications Technology (NICT), Tokyo, Japan. He is currently the Technology Manager with ITRI. He has authored and coauthored 35 refereed journal articles and 40 conference papers. He holds over 70 patents, including U.S., Taiwan, China, and EU patents. His published articles have been cited over 1700 times with an H-index of 23 in Google Scholar.

Dr. Li served as an International Steering Committee Member for ISAP, from 2019 to 2022; and an AdCom Member for the Institute of Antenna Engineers of Taiwan, in 2014 and 2015, and from 2018 to 2023. He also served as a member for the Judge Panel of the National Terminal Antenna Design Competition, organized by the Taiwan Ministry of Economics, from 2014 to 2023. He received the Young Scientist Award in 2007 ISAP and the Best Paper Award (APMC Prize) in 2008 APMC. He has been a principal investigator or a co-principal investigator of many research projects in ITRI and has received numerous recognitions, including the First Prize of the Outstanding Research Award of ITRI, in 2010; the Solar Industrial Award (SIA) of Europe, in 2011; the Outstanding Innovation Award of ITRI, in 2013; the Second Prize of the Outstanding Research Award of ITRI, in 2014; the 2015 Research and Development 100 Award Finalist of the U.S.; the Outstanding Innovation Award of ITRI, in 2017; the First Prize of the Outstanding Industrialization Award of ITRI, in 2017; the Second Prize of the Outstanding Industrialization Award of ITRI, in 2020; and the Third Prize of the Outstanding Industrialization Award of ITRI, in 2021. He also received the Outstanding Lecturer Award of ITRI, in 2013; the International Paper Award of ICL of ITRI, in 2020; and the Annual Paper Award of ITRI, in 2023. He also served as the Chair for IEEE AP-S Tainan Chapter, from 2021 to 2022.